Available online at www.sciencedirect.com
SCIENCE DIRECT®
Journal of Solid State Chemistry 179 (2006) 2252–2257
JOURNAL OF SOLID STATE CHEMISTRY
www.elsevier.com/locate/jssc

Thermoelectric properties and microstructure of Mg_3Sb_2

Cathie L. Condron[a], Susan M. Kauzlarich[a,*], Franck Gascoin[b,c], G. Jeffrey Snyder[b,c]

[a]Department of Chemistry, University of California Davis, One Shields Avenue, Davis, CA 95616, USA
[b]California Institute of Technology, Materials Science, 1200 East California Boulevard, Pasadena, CA 91125, USA
[c]Jet Propulsion Laboratory/California Institute of Technology, 4800 Oak Grove Drive, Pasadena, CA 91109, USA

Received 23 November 2005; received in revised form 11 January 2006; accepted 15 January 2006
Available online 28 February 2006

Dedicated to the occasion of the 75th birthday of Prof. Hans Georg von Schnering

Abstract

Mg_3Sb_2 has been prepared by direct reaction of the elements. Powder X-ray diffraction, thermal gravimetric, differential scanning calorimetery, and microprobe data were obtained on hot pressed samples. Single phase samples of Mg_3Sb_2 were prepared and found to contain oxygen at the grain boundaries and to lose Mg and oxidize at temperatures above 900 K. Thermoelectric properties were characterized by Seebeck, electrical resistivity, and thermal conductivity measurements from 300 to 1023 K, and the maximum zT was found to be 0.21 at ~875 K.

Keywords: High temperature thermoelectric; Calorimetry; Mg_3Sb_2; Thermoelectric; Zintl phase; Zintl; Composite thermoelectric; Antimonide

1. Introduction

Thermoelectric materials devices have gained renewed interest for environmentally benign power generation [1–3]. If sufficiently efficient, thermoelectric devices can be developed to utilize waste heat sources, such as geothermal vents or automotive exhaust heat, to produce electrical power. Such power generation would require minimal amounts of fossil energy consumption, and would produce virtually no harmful emissions.

A good thermoelectric material requires the combination of high electrical conductivity (σ) or low electrical resisitivty (ρ), low thermal conductivity (κ), and high thermopower or Seebeck coefficient (S), ultimately resulting in a high figure of merit ($zT = S^2T/\rho\kappa$, where T is temperature) [3]. Materials that best meet these requirements are typically heavily doped, small band-gap semiconductors or semimetals. Such materials provide a balance between the high Seebeck coefficient of semiconductors and the low electrical resistivity of metals.

The Zintl phase Mg_3Sb_2, which crystallizes with the inverse α-La_2O_3 structure type (P-3m1, $Z = 1$) [4,5] has been investigated in hopes of achieving a high figure of merit for high temperature applications. Mg_3Sb_2 was first recognized as a potential thermoelectric material by Bredt and Kendall [6], but this work was hampered by difficulties with sample preparation. As a follow up, Verbrugge and Zytveld showed that Mg–Sb alloys were found to be similar to Pb–Te alloys with the advantages of a smaller mass density and a lower vapor pressure [7]. However, their investigation showed that Mg–Sb, at concentrations just off stoichiometry, gave a zT~0.1, implying that these materials are only marginally interesting for commercial applications, and suggested that on—stoichiometry samples with the addition of third and fourth element impurities, may improve the properties of this material [7]. Motivation for this investigation was provided by a report by Kajikawa et al. [8], who performed a similar study on Mg_3Sb_2 and Mg_3Bi_2 in the medium temperature range 300–773 K. Kajikawa et al. estimated a promising dimensionless figure of merit, zT, for Mg_3Sb_2 of 0.55 at 600 K. The reported zT, along with an improved compatibility factor for segmented TE devices [9] provided

*Corresponding author. Fax: +1 530 752 8995.
E-mail address: smkauzlarich@ucdavis.edu (S.M. Kauzlarich).

0022-4596/$ - see front matter © 2006 Elsevier Inc. All rights reserved.
doi:10.1016/j.jssc.2006.01.034

incentive for more detailed studies. In the paper by Kajikawa et al. the increased zT was attributed to the microstructure induced by hot pressing, however, no microstructure data were presented. In addition, there was no analysis given of the powder X-ray diffraction data. Further motivation was provided by recent reports that $Ca_xYb_{1-x}Zn_2Sb_2$, which share the same structure as Mg_3Sb_2, have promising zT values, but lack stability at high temperatures [10].

Powder samples of Mg_3Sb_2 were synthesized by direct reaction of the elements Mg and Sb for high temperature analysis. The microstructure and phase stability along with thermoelectric properties analysis in the temperature range 300–1373 K will be presented and discussed.

2. Experimental section

2.1. Sample preparations

Mg_3Sb_2 was synthesized by direct reaction of the elements Mg (Aldrich, 99.98%), and Sb (Alfa Aesar, 99.9999%). The stoichiometric reaction always showed unreacted Sb in the X-ray powder diffraction of the final product. Therefore, excess of Mg was added to the reaction to compensate for the unreacted Sb. It was found that the minimum amount of excess Mg needed to obtain an X-ray powder diffraction pattern of pure Mg_3Sb_2 was 3.5 Mg to 2 Sb. Elements were loaded into boron nitride crucibles that were capped, placed in a fused silica tube, and sealed under 1/5 atm Ar. The reaction vessel was heated to 1073 K for 7 days. After 7 days the furnace was turned off and allowed to cool to room temperature before reaction vessels were removed. The reaction product was a mixture of powder, polycrystalline material and single crystals. In order to obtain a dense sample, finely ground polycrystalline powder was hot-pressed in high-density graphite dies (POCO). The hot-pressing was conducted at a pressure of about 20,000 psi and at 873 K for 1.5 h under argon atmosphere. A cylinder about 10 mm long and 8 mm in diameter was thus obtained. Its density (calculated from measured dimensions and weight) was found to be about 99% of the theoretical density.

2.2. Characterization

X-ray powder diffraction data were collected with an INEL CPS 120, which performs the simultaneous collection of 2θ diffracted X-rays over 120°. Data acquisition was performed with WinAcq software.

Microprobe analysis were performed on polished pressed pellets placed on carbon tape. The samples were placed in a Cameca SX100 electron microscope equipped with a wavelength-dispersive spectrometer. The microprobe was operated at 15 nA beam current at 20 keV accelerating potential. Net elemental intensities for Sb and Mg were determined with respect to pure elemental calibration standards that were polished before the measurement to ensure the elements were not oxidized. Totals for all analyses were 100%.

A Netzsch Thermal Analysis STA 409 cell, equipped with a TASC 414/2 controller and PU 1.851.01 power unit was used to evaluate the thermal properties of Mg_3Sb_2 between 298 and 1373 K. After a baseline was established, pieces of the hot pressed pellet (30–50 mg) were placed in alumina crucibles and heated under vacuum at 2 K/min with an acquisition rate of 5 pts/K.

2.3. Thermoelectric properties measurements

Samples in the form of discs (typically 1 mm thick and 8 mm diameter slice) were cut from the cylinder using a diamond saw for electrical and thermal transport properties, while the Seebeck coefficient measurement was performed on the remaining cylinder. All these physical properties were measured between room temperature and 1023 K.

The electrical resistivity (ρ) was measured using the van der Pauw technique with a current of 100 mA using a special high temperature apparatus [11]. The Seebeck coefficient (S) was measured using a high temperature light pulse technique [12]. Heat capacity and thermal diffusivity were measured using a flash diffusivity technique. The thermal conductivity (κ) was then calculated from the experimental thermal diffusivity and calculated values for density and heat capacity of Dulong–Petit.

3. Results and discussion

Fig. 1 shows the structure of Mg_3Sb_2 along with the X-ray powder diffraction pattern of the product formed

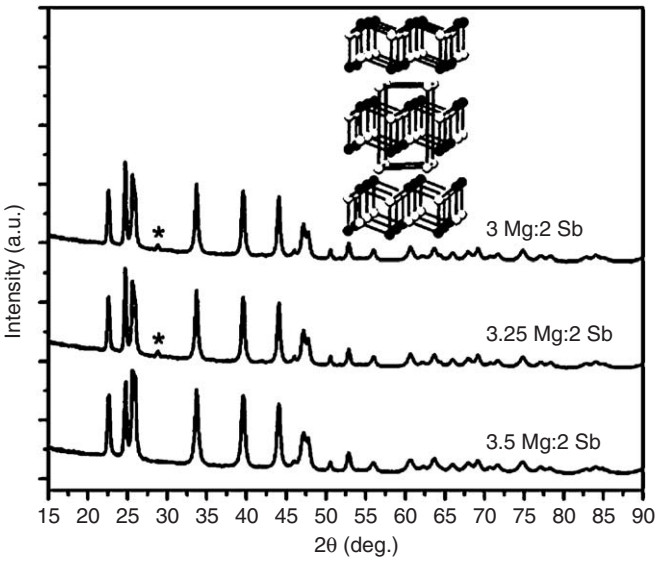

Fig. 1. Powder X-ray diffraction patterns of different reaction stoichiometries for the synthesis of Mg_3Sb_2. *(012) reflection of Sb. The inset illustrates the crystal structure of Mg_3Sb_2 along the [100] direction (white = Mg, black = Sb). Crystal structure generated by Ozawa and Kang [17].

from the reaction stoichiometries $(3+x)$ Mg:2 Sb ($x = 0$, 0.25, and 0.5). All diffraction peaks from the products of the reactions with $x = 0$ and 0.25 could be indexed to Mg_3Sb_2 (inverse α-La_2O_3 structure type) except the peak attributed to the most intense reflection (012) of Sb. The product formed from the reaction with $x = 0.5$ could be completely indexed to Mg_3Sb_2.

The TG (mass%), and DSC versus temperature for a piece of the hot pressed pellet of Mg_3Sb_2 prepared with stoichiometry $x = 0.5$ are shown in Fig. 2. The mass% decreases gradually up to 900 K then drops by approximately 17%. This weight loss is due to the Mg leaching out of the structure at elevated temperature, as Mg was found completely covering the sample crucible lid when it was removed from the instrument, with a fine grey powder remaining in the crucible itself. These results were reproduced by sealing a piece of the pressed pellet in a quartz ampoule and subsequently heating to 1423 K over several hours. The X-ray powder diffraction pattern of the resulting grey powder obtained from TGA/DSC is given in Fig. 3, and is the same as the X-ray powder diffraction pattern found after heating the sample under vacuum to 1423 K. The pattern can be indexed as a combination of MgO, Sb, and Mg_3Sb_2. The X-ray powder diffraction pattern is similar to that provided by Kajikawa et al. indicating that hot pressing at elevated temperatures (above 900 K) gives an inhomogeneous product [8]. The sample prepared by Kajikawa et al. is likely an Mg_3Sb_2/Sb/MgO composite and the measured properties will depend strongly on the relative composition of these phases.

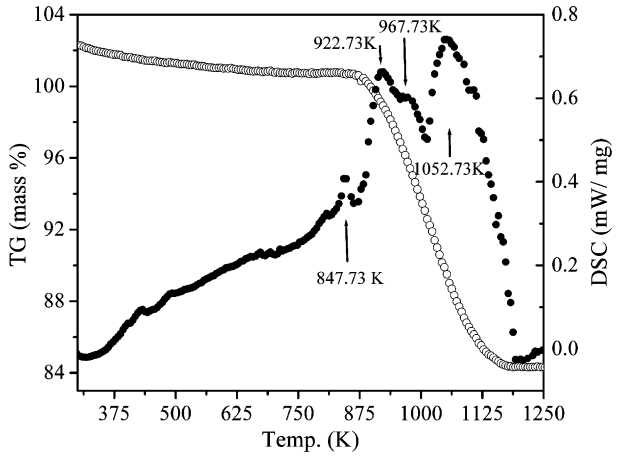

Fig. 2. TG (○) and DSC (●) as a function of temperature for Mg_3Sb_2. Data were obtained by heating at a rate of 2 K/min under vacuum.

The DSC versus temperature displays a broad exotherm from 300 to 800 K, and several prominent exothermic transitions in the temperature range of 800–1200 K. The broad exotherm is attributed to the oxidation of the sample, with the phase change and decomposition occurring above the sharp exotherm at 800 K. The exotherms at 922, 967, and 1052 K are attributed to subsequent crystallization.

Fig. 4 displays the back-scattered electron image (BSEI), and X-ray maps of Mg, Sb, and O, respectively, for the polished pressed pellet of Mg_3Sb_2. The BSEI as well as the X-ray maps for Mg and Sb, show that the main phase, Mg_3Sb_2, is uniform with no oxygen. The bright and dark regions in the BSEI image indicate a different phase is present at the grain boundaries. The Mg X-ray map is also uniform with light and dark regions in a similar pattern as observed in the BSEI image. The light areas indicate a higher concentration of Mg than the main phase, and the dark areas indicate a lower concentration of Mg. Similarly, the Sb X-ray map is mostly uniform with light regions that are in the same pattern as the dark regions observed in the Mg X-ray map. The very bright regions in the BSEI image indicate a higher concentration of Sb in these regions. The O X-ray map shows that the oxygen content occurs at the grain boundaries with Mg. Fig. 4 displays the BSEI, and X-ray maps of Mg, Sb, and O, respectively, for the powder sample recovered from the crucible after TG/DSC. The BSEI image in Fig. 5 shows large regions of inhomogeneity. The Mg and O X-ray maps clearly show the sample has degraded and is mostly oxidized with isolated regions of Sb as seen in the Sb X-ray map. This is consistent with the powder pattern given in Fig. 3.

The temperature dependence of the electrical resistivity and Seebeck coefficient, S, for hot pressed pellets of Mg_3Sb_2 are shown in Figs. 6(a) and (b), respectively. The Seebeck coefficient increases with temperature up to 550 K,

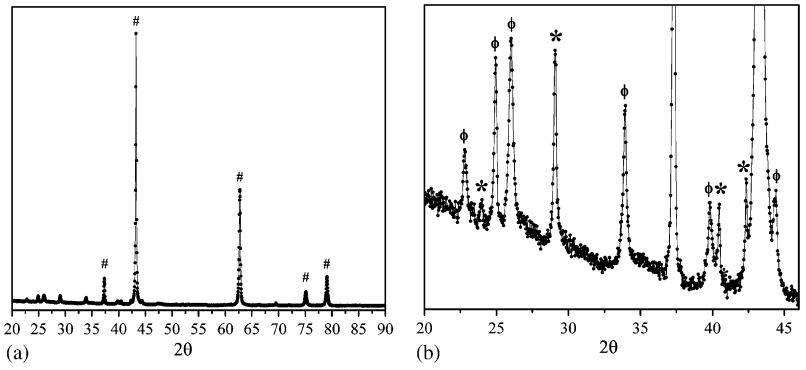

Fig. 3. (a) Powder X-ray diffraction pattern of fine grey powder found after TG/DSC (# = MgO). (b) Expanded view between 20 and 50 2θ showing that Sb (*), and Mg_3Sb_2 (ϕ), are present along with MgO.

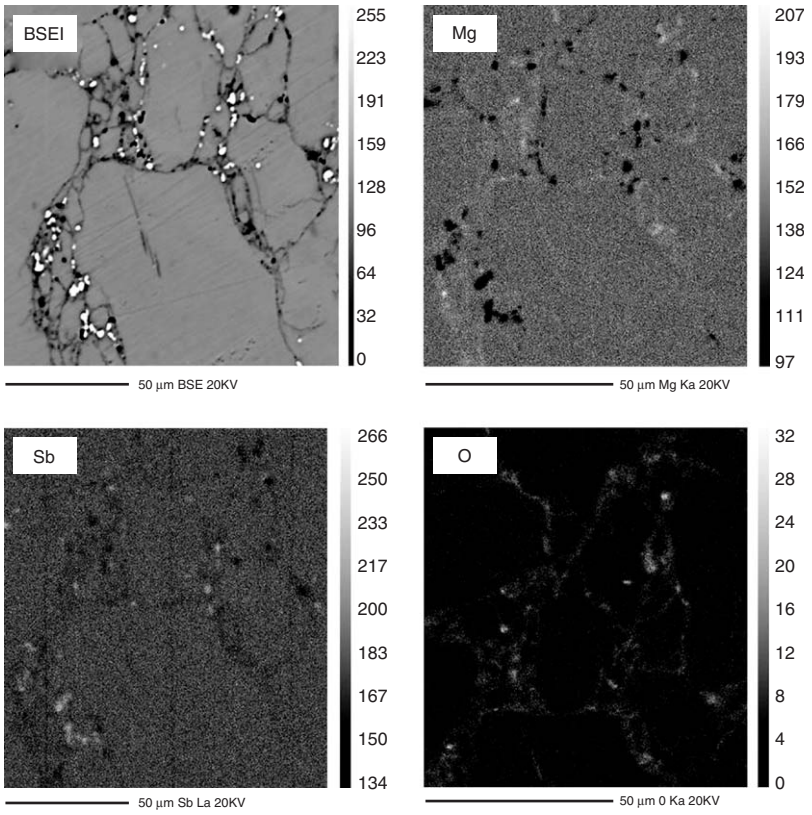

Fig. 4. Back-scattered electron image (BSEI) of Mg_3Sb_2, and X-ray maps at 20 kV of Mg, Sb, and O, respectively, for the polished pressed pellet of Mg_3Sb_2. Scale bar is 50 μm.

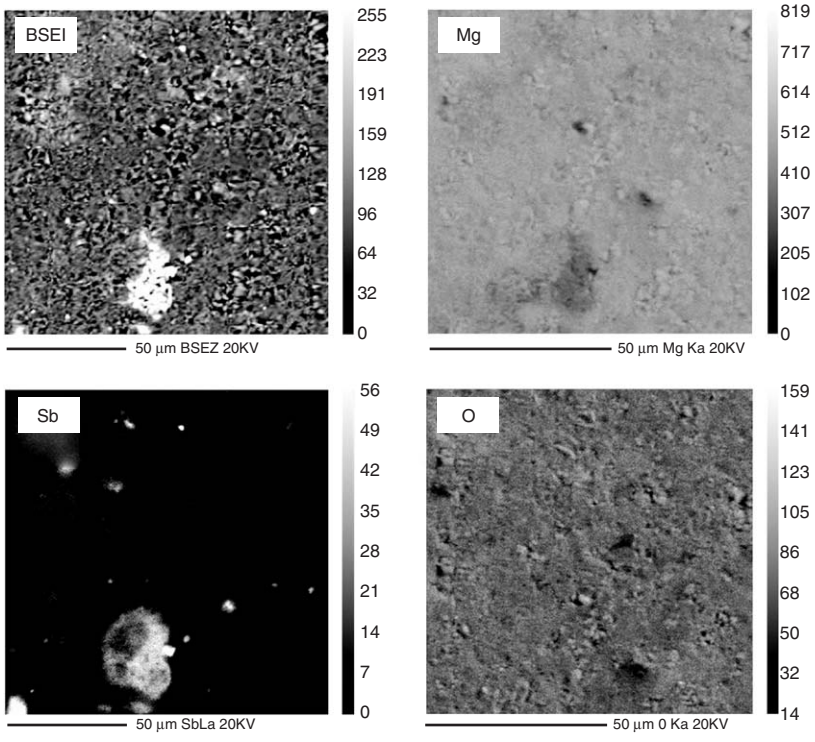

Fig. 5. Back-scattered electron image (BSEI), and X-ray maps at 20 kV of Mg, Sb, and O, respectively, for the resulting grey powder found after heating under vacuum to 1423 K. Scale bar is 50 μm.

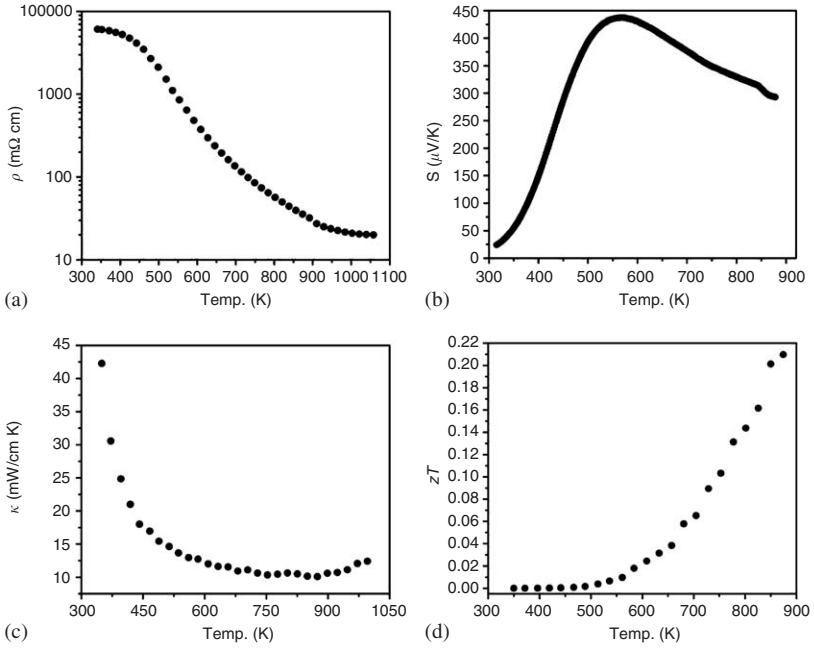

Fig. 6. Shows the temperature dependence of the (a) resistivity, (b) Seebeck coefficient, (c) thermal conductivity, and (d) dimensionless figure of merit for Mg_3Sb_2 hot pressed and sintered at 873 K.

then begins to decrease in temperature, and the electrical resitivity decreases with increasing temperature, characteristic of semiconducting behaviour. In comparing our data with that presented by Kajikawa et al. [8] we note that both the resistivity and Seebeck coefficient of our sample follow the same trends, however, we do not obtain the same values. For example, our maximum Seebeck coefficient of ~445 μV/K at ~550 K falls in between the values of the sample sintered at 1273 K, and those sintered at 1213 and 1253 K reported by Kajikawa et al. Similarly, the electrical resisitivy of our sample is higher and hence electrical conductivity is lower than all three samples reported by Kajikawa et al. Fig. 7 provides conductivity versus temperature data in order to more easily compare this work with that of Kajikawa et al. The differences in conductivity and Seebeck between this work and Kajikawa are presumably because our sample was hot pressed and sintered at 873 K which is much lower than any of the samples prepared by Kajikawa et al. By hot pressing at 873 K we are able to keep Mg_3Sb_2 stoichiometric and free from oxidation, with the exception of very small amounts at the grain boundaries (Fig. 4), giving rise to a higher resistivity and lower Seebeck coefficient. The microstructure of the pressed pellet is particularly important for the electrical resistivity. The MgO at the grain boundaries should increase the resistivity while the presence of Sb should decrease the resistivity. Neither MgO or Sb should have a significant effect on the Seebeck coefficient. The relative amounts of these two phases will greatly affect the resistivity, and perhaps the lower resistivity values reported by Kajikawa et al. are due to increased amounts of Sb. It might be useful to have a BSEI study of the grain boundaries of samples prepared under the same condictions as Kajikawa et al. in order to correlate better the effect on thermoelectric properties.

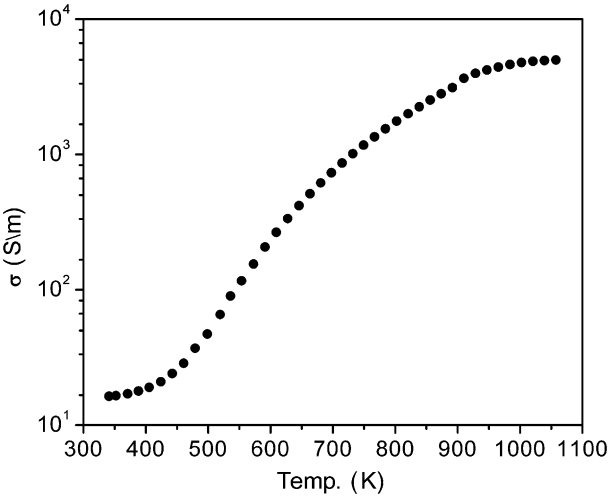

Fig. 7. Temperature dependence of the electrical conductivity.

In any case, some general conclusions concerning the thermoelectric behaviour of Mg_3Sb_2 can be drawn: As indicated in Ioffe's theory [13], the temperature dependence of the electrical conductivity suggests the Seebeck coefficient should decrease with increasing temperature. This, however, contradicts the experimental results in the temperature range 300–550 K, indicating the behaviour of the Seebeck coefficient is highly affected by ionizing impurity scattering, which reduces the value of the Seebeck coefficient.

Furthermore, in accordance with the TG data presented earlier, by hot pressing at the temperatures used by Kajikawa et al. Mg_3Sb_2 will have degraded into a combination of Mg_3Sb_2, Sb, and MgO. This hypothesis is supported by the X-ray powder pattern presented by Kajikawa et al. which is similar to the one provided in Fig. 3, showing a mix of Mg_3Sb_2, Sb, and MgO.

Fig. 6(c) shows the thermal conductivity versus temperature for hot pressed pellets of Mg_3Sb_2. There are two components to the thermal conductivity, the electronic component (κ_{el}) depends on the electrical conductivity and can be estimated using the Wiedemann–Franz law, $\kappa_{el} = L\sigma T$ (where L is the Lorenz number, σ is the electrical conductivity, and T is temperature). The second component is the lattice component and depends on structural details such as structure type and disorder. Thermal conductivity of crystalline solids commonly displays $1/T$-type of temperature dependence. Nearly temperature-independent thermal conductivities are indicative of disordered and amorphous materials [14]. As shown in Fig. 6(c), the thermal conductivity of Mg_3Sb_2 is temperature independent above 500 K and agrees well with the value previously reported (4.2 W/mK, at room temperature) [15], as well as the data presented by Kajikawa et al. [8]

The temperature dependence of the dimensionless figure of merit, $zT = (S^2T)/\rho\kappa_{total}$ is displayed in Fig. 6(d) and increases with temperature to a maximum of 0.21 at ~875 K. Therefore, although the thermal conductivity is reasonably low and comparable to those of good thermoelectric materials [16], the zT of these Mg_3Sb_2 samples is too low for thermoelectric applications.

4. Summary

Mg_3Sb_2 has been prepared by direct reaction of the elements and characterized using powder X-ray diffraction. Single phase samples of Mg_3Sb_2 were hot pressed at about 20,000 psi and at 873 K for subsequent analysis. Microprobe analysis revealed that the hot pressed pellets contained oxygen at the grain boundaries, and TG/DSC shows that the hot pressed pellets lose Mg and oxidize at temperatures above 900 K. Thermoelectric properties were characterized by Seebeck, electrical resistivity, and thermal conductivity measurements from 300 to 1023 K, and the maximum zT was found to be 0.21 at ~875 K. Since the zT of Mg_3Sb_2 is very low, and degrades above 900 K, the pure phase is not a good candidate for thermoelectric applications. Further investigation of the composite phase, MgO/Mg_3Sb_2/Sb, along with the correlation of microstructure to thermoelectric properties might be worthwhile for optimization of this system.

Acknowledgments

We thank Alexandra Navrotsky (University of California Davis) for the use of the Netsch 409 TG/DSC instrument. Portions of this work were carried out by the Jet Propulsion Laboratory, California Institute of Technology, under contract with NASA. This research was funded by NASA and NSF.

References

[1] X. Ma, S.B. Riffat, Appl. Therm. Eng. 23 (2003) 913.
[2] G. Chen, G. Dresselhaus, M.S. Dresselhaus, J.P. Fleurial, T. Caillat, Int. Mater. Rev. 48 (2003) 45.
[3] C. Wood, Rep. Prog. Phys. 51 (1988) 459.
[4] E. Zintl, E. Husemann, Z. Phys. Chem. 21B (1933) 138.
[5] M. Martinez-Ripoll, A. Haase, G. Brauer, Acta Cryst. B 30 (1974) 2006.
[6] J.H. Bredt, L.F. Kendall, Proceedings—IEEE/AIAA (1966).
[7] D.M. Verbrugge, J.B.J. Van Zytveld, Non-Cryst. Solids 156–158 (1993) 736.
[8] T. Kajikawa, N. Kimura, T. Yokoyama, in: Proceedings of the 22nd International Conference on Thermoelectrics, 2003, p. 305.
[9] G.J. Snyder, Appl. Phys. Lett. 84 (2004) 2436.
[10] F. Gascoin, S. Ottensmann, D. Stark, S.M. Haile, G.J. Snyder, Adv. Funct. Mater. 15 (2005) 1860.
[11] J.A. McCormack, J.P. Fleurial, Mater. Res. Soc. Symp. Proc. 234 (1991) 135.
[12] C. Wood, D. Zoltan, G. Stapfer, Rev. Sci. Instrum. 56 (1985) 719.
[13] A.F. Ioffe, in: Semiconductor Thermoelements and Thermoelectric Cooling, 1957.
[14] C.M. Bhandari, D.M. Row, Thermal Conduction in Semiconductors, Wiley Eastern Limited, New Delhi, 1988.
[15] F.S. Galasso, Structure and Properties of Inorganic Solids, Pergamon Press Inc., Oxford, 1970, p. 157.
[16] G.J. Snyder, M. Christensen, E. Nishibori, T. Caillat, B.B. Iversen, Nat. Mater. 3 (2004) 458.
[17] T.C. Ozawa, S.J. Kang, J. Appl. Crystallogr. 37 (2004) 679.